

# Multiple-object input in nonlinear correlation

Tuvia Kotzer, Joseph Rosen, and Joseph Shamir

Multiple-object input to the recently introduced phase-extraction correlator may cause difficulties owing to interference effects. Similar effects have been observed previously in the nonlinear joint transform correlator. It is shown theoretically and by computer simulations that these effects are seldom observable in practice, and even then they can be substantially reduced by employing a proper space-variant threshold. The implementation of this scheme by a hybrid electro-optical architecture is also explained briefly and demonstrated. The results presented permit manipulation of information (spectral phase) that was previously believed to be contaminated beyond recovery.

## 1. Introduction

Recently we presented<sup>1</sup> an optical system that performs correlations based purely on the phase distribution in the Fourier-transform (FT) plane<sup>2,3</sup> (phase-only correlation). The performance of this phase-extraction correlator (PEC) was demonstrated<sup>4</sup> to be superior to its linear counterpart except for some special cases of inputs with multiple identical objects. It was indicated that good performance could be restored for these cases as well by modifying the PEC through the use of a spatially varying threshold.

Our purposes are to analyze further the problem of multiple-object inputs, to determine its extent, and to derive procedures for its alleviation. The analysis presented here, although developed originally for the PEC, is quite general and can be extended for the treatment of other aspects of signal processing in which phase extraction is involved. Specifically, the analysis may be applied to the nonlinear joint transform correlator (JTC)<sup>5</sup> and its observed problems, such as the binarization of the JTC spectrum.<sup>6</sup> Also, it may be applied for the reconstruction of signals from their Fourier phase under conditions that were previously believed to cause signal irrecoverability.<sup>7</sup>

After a short review of earlier research in Section 2 we present a comprehensive analysis of the multiple-object problem in Section 3 that is based on a statistical model treated in Appendix A. Modification of the PEC to a space-variant threshold PEC, the SVTPEC, is described in Section 4, and we demon-

strated how it can alleviate problems that may arise during the use of the simple PEC. In Section 5 the theoretical predictions are confirmed by computer simulations, and laboratory experiments are described in Section 6. It should be noted that the SVTPEC yields results that were not foreseen,<sup>7,8</sup> by manipulating the Fourier phase only at those frequency regions at which the amplitudes of the input spectral distributions are not less than some input-dependent threshold. Conclusions are given in Section 7.

## 2. Phase-Extraction Processing: Review

The system architecture is presented in Fig. 1. The point nonlinearity operator  $N_l$  is defined with the help of a general function  $R(u, v) = |R(u, v)| \exp j\phi(u, v)$  by the relation

$$N_l[R(u, v)] = \begin{cases} |R(u, v)|^l \exp j\phi(u, v), & 0 \leq l \leq 1, \text{ for } R(u, v) \neq 0 \\ 1 & \text{otherwise} \end{cases} \quad (1)$$

Concentrating on  $l = 0$ , we deal with the extraction of the phase function from  $R(u, v)$ . The input function  $q(x, y)$  is Fourier transformed to  $Q(u, v)$ , from which the phase is extracted by Eq. (1), yielding  $Q'(u, v)$ . The filter function  $p(x, y)$  undergoes a transformation identical to the input function  $q(x, y)$ . The two phase functions are multiplied, and the result  $G'(u, v)$  is inverse-Fourier transformed to yield the correlation output  $C(x, y)$ . Note that in the classical case,  $P(u, v)$  in Fig. 1 is the matched filter of the specific object to be detected and  $P'(u, v)$  is the phase-only MF (POMF).<sup>9</sup>

By the nature of the PEC, the higher frequencies of

The authors are with the Department of Electrical Engineering, Technion-Israel Institute of Technology, Haifa 32000, Israel.

Received 23 April 1992.

0003-6935/93/111919-14\$05.00/0.

© 1993 Optical Society of America.

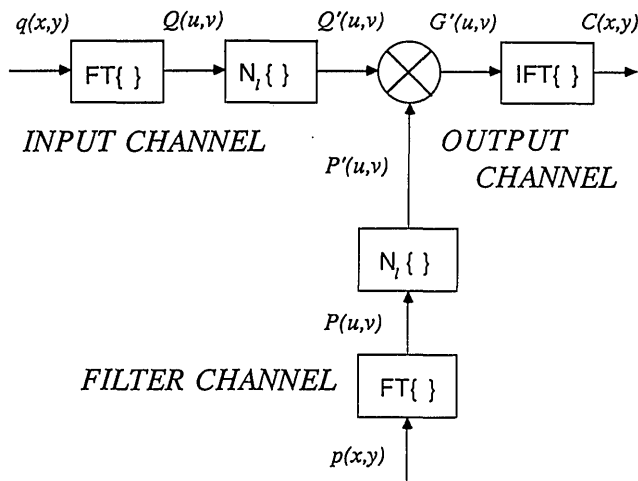


Fig. 1. Block diagram of the symmetric nonlinear pattern-recognition system: FT and IFT denote the Fourier transform and its inverse, respectively;  $q(x, y)$  and  $p(x, y)$  are the input and filter functions, respectively;  $N_l$  is a point nonlinearity, operating on the function  $R(u, v)$ , and is defined by Eq. (1).

the input are amplified, enhancing discrimination capabilities. In fact, it was shown<sup>4</sup> that the output correlation response to an input consisting of one and two objects, to which the filter is matched, are delta functions at the correct positions with subsidiary low-amplitude grass, or noise, in the two-object input case. For multiple-object inputs, however, the situation is more complicated. This is the main subject here and is examined in Section 3.

### 3. Phase Extraction for Multiple-Object Input

When several objects are presented in the input plane of a coherent optical processor their FT's are superposed coherently over the FT plane. As long as only linear processes are considered, this superposition has no harmful effects. However, if a nonlinear process takes place at the FT plane, interference effects may manifest themselves, resulting in an impairment of system performance. Since phase extraction is such a nonlinear process, one should expect difficulties, as indeed was indicated by simulation results<sup>4,6</sup> when four objects were presented at regular intervals.

For convenience and clarity we describe in detail objects positioned along one linear dimension only, but generalization to two dimensions is straightforward. Assume that we have  $N$  objects  $a(x)$  in the input plane, each centered at  $x_i$ , where  $i = 1, \dots, N$ . The input distribution can be written in the form

$$q(x) = \sum_{i=1}^N a(x - x_i), \quad (2)$$

with its FT obtained by

$$Q(u) = |A(u)| \exp j\phi(u) \sum_{i=1}^N \exp j2\pi u x_i, \quad (3)$$

where  $A(u) = \mathcal{F}[a(x)]$  and  $\phi(u) = \arg[A(u)]$ . Taking  $l = 0$  in Eq. (1), we obtain the phase distribution of the input pattern as

$$Q'(u) = \exp j\phi(u) \frac{\sum_{i=1}^N \exp j2\pi u x_i}{\left| \sum_{i=1}^N \exp j2\pi u x_i \right|}. \quad (4)$$

Assuming that a filter function  $p(x)$  is matched to  $a(x)$ , we have the phase distribution extracted from the filter function, obtained by

$$P'(u) = \exp -j\phi(u). \quad (5)$$

Thus, before performing the inverse-Fourier transform (IFT) we have the distribution

$$c(u) = P'(u)Q'(u) = \frac{\sum_{i=1}^N \exp j2\pi u x_i}{\left| \sum_{i=1}^N \exp j2\pi u x_i \right|}. \quad (6)$$

Hence the output correlation function  $C(x)$  is obtained by the convolution theorem and is

$$\begin{aligned} C(x) &= \mathcal{F}^{-1}c(u) = \mathcal{F}^{-1}\left(\sum_{i=1}^N \exp j2\pi u x_i\right) \\ &\quad * \mathcal{F}^{-1}\left(\frac{1}{\left|\sum_{i=1}^N \exp j2\pi u x_i\right|}\right) \\ &= \sum_{i=1}^N \delta(x - x_i) * \mathcal{F}^{-1}\left(\frac{1}{[N + D(u)]^{1/2}}\right) \\ &= \sum_{i=1}^N \delta(x - x_i) * V(x), \end{aligned} \quad (7)$$

where

$$\begin{aligned} V(x) &= \mathcal{F}^{-1}\left(\frac{1}{[N + D(u)]^{1/2}}\right), \\ D(u) &= \sum_{i=1}^N \sum_{l=1, l \neq i}^N \exp j2\pi u (x_i - x_l) \end{aligned} \quad (8)$$

are functions of the input-object positions alone, with no dependence on their shape or size and  $*$  denotes the convolution operator. If the positions of the input objects are random, then  $D(u)$  is derived from many uncorrelated terms, and the function  $V(x)$ , defined by Eq. (8), describes a random process. Under these circumstances we expect  $V(x)$  to be comparable with  $\delta(x)$ , as is confirmed in the detailed mathematical analysis presented in Appendix A. If a large number of objects, for which the filter is matched, are randomly distributed along  $x$ , then  $x_i$  can be considered a random variable, and  $V(x)$ , which

we call the modulating term, has  $\delta(x)/\sqrt{N}$  as its mean, and its variance is of the order of  $1/N$ . This is a narrow, spatially confined modulating term.

The important result of the above considerations is that the response of the PEC to the input obtained by Eq. (2) is, with  $x_i$  as a random variable,

$$C(x) \approx \frac{\sum_{i=1}^N \delta(x - x_i)}{\sqrt{N}}. \quad (9)$$

This is a series of delta functions at the correct positions with a relatively low normalized variance [see relation (A19)]. To first approximation, all the energy in the correlation plane is uniformly distributed among the  $N$  correlation peaks.

The above results were derived for objects matched to the filter function that were randomly scattered over the input plane, and they indicate that the performance of the PEC is not impaired by such an input. Naturally, if many objects that are not matched to the filter are present too, they will not correlate, regardless of their arrangement in the input plane, and they will leave the proper correlation peaks intact, as is demonstrated in Section 5.

Our derivation, however, breaks down if statistical considerations of random variables are not applicable. An extreme case consists of identical objects that are matched to the filter and arranged in a regular array. Such an array, in one dimension, can be represented by the  $x_i$  values in Eq. (2), obtained by  $x_i = x_1 + (i - 1)b$  ( $i = 1, \dots, N$ ), with the modulating function [Eq. (8)] obtained in the form

$$V(x) = \mathcal{F}^{-1} \left[ \left| \frac{\sin(\pi ub)}{\sin(\pi uNb)} \right| \right]. \quad (10)$$

The primary contributions to Eq. (10) are from points at which  $\sin(\pi ub)/\sin(\pi uNb)$  has poles. Since there is an infinite number of these, the IFT is similar to a train of delta functions multiplied by some envelope function. Therefore  $V(x)$  is a wideband signal, and hence the system is no longer shift invariant. Each object affects the correlation response of all the other objects in an essentially unpredictable way. This results in poor performance of the PEC for a regular array of equally spaced identical input objects, as has been indicated by computer simulations.<sup>4</sup>

To support our results, we generated  $V(x)$  with 8 objects separated regularly from each other by 4 pixels and two random distributions of 50 and 5 identical objects along a one-dimensional line. The respective forms of  $|V(x)|$  obtained are shown in Fig. 2. The spatial width of  $|V(x)|$ , as observed in Fig. 2(a), is much larger than the separation between the objects (4 pixels), and hence the correlation response at the center of each object is strongly affected by the presence of the other objects in the input plane. In contrast, in the case of a random distribution [Fig. 2(b)],  $V(x)$  is essentially a delta function that leads to 1-pixel-wide peaks in the true positions. It is inter-

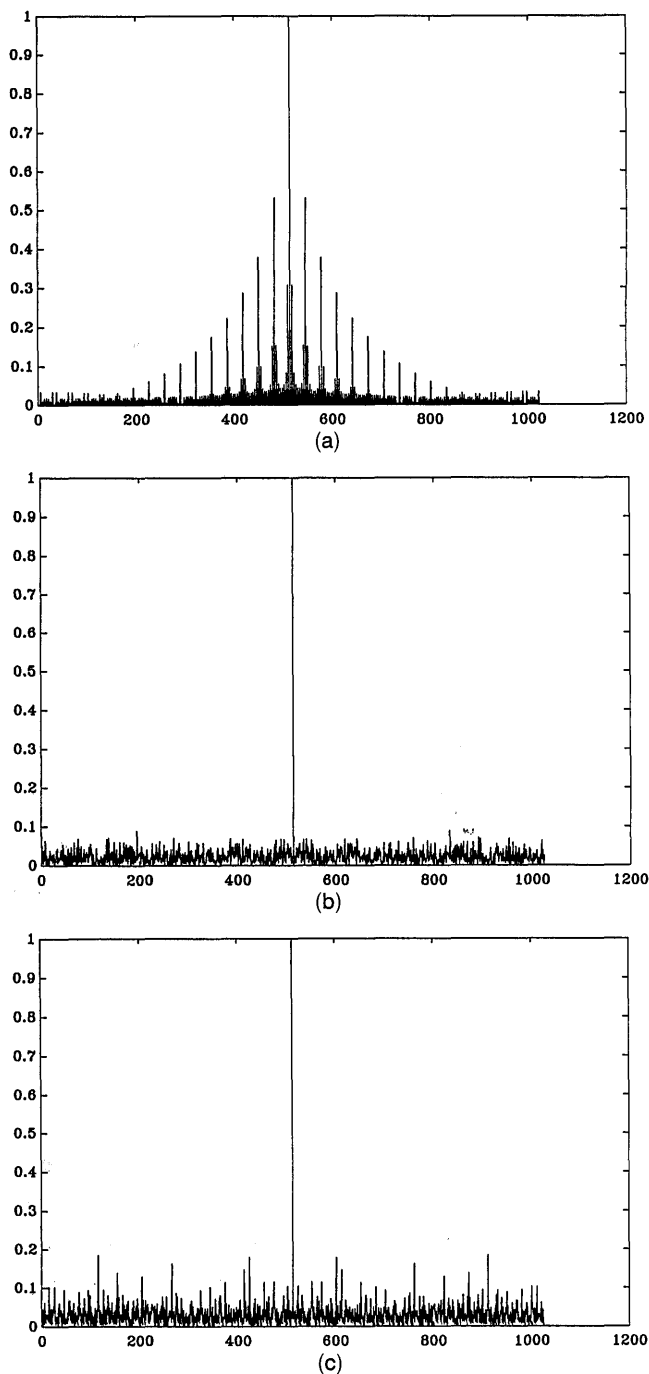


Fig. 2. Distribution of  $V(x)$  for the following: (a) 8 objects equally spaced (4 pixels apart), (b) 50 objects randomly scattered in the input plane, and (c) 5 objects randomly scattered in the input plane.

esting to note that, although the mathematical analysis for the random input in Appendix A seems to require a large  $N$  for the analysis to be valid, Fig. 2(c) indicates that, even for  $N = 5$ , the results are functionally correct. Nevertheless, we observed that the level of the noise in  $V(x)$  increased as the number of randomly spaced objects decreased. This is in good correspondence with relation (A18), in which we refer to the noise  $\sigma$  as the low-amplitude grass

surrounding the delta functions in Figs. 2(b) and 2(c). Also, it should be emphasized that, even for a similar number of objects in the input [Figs. 2(a) and 2(c)], the modulating term can be substantially different, depending on the arrangement of the objects in the input.

In a separate study, in which 50 identical objects were placed randomly in a two-dimensional plane, we obtained the ratio of minimal true peak/maximal true peak equal to 0.8 (in intensity), implying small peak variance, and the ratio of minimal true peak/maximal false peak equal to 53, implying small sidelobes (noise). This is in accordance with our analysis regarding the performance of the PEC when objects are scattered randomly in the input plane.

To recapitulate this section, we have demonstrated that the high-level performance of the PEC was preserved for randomly distributed multiple objects in the input plane as for a single object.<sup>1</sup> However, the PEC exhibited poor performance, at least theoretically, when several identical input objects were arranged in a regular array. The question is, what happens when the input distribution lies between these extremes? Simulations (Section 5) indicate that the PEC performs well even for a pseudo random distribution, and narrow peaks of approximately identical strengths with low sidelobes are generated at the center position of the objects. Basically, the PEC performs well for any nonpatterned input, in which the linear phases generated by the displacement of the objects do not modulate the amplitude distribution of the FT of the input to a large extent.

Study of the random case indicates that the problem of the PEC can be mitigated by eliminating the sidelobes. Two obvious ways to achieve this objective are as follows:

(1) One can add low-amplitude noise to the input. When this is done, the pattern of the low-amplitude sidelobes in the spatial frequency plane, which is the primary reason for the impairment of the performance of the PEC (generated by the sum of the linear phases), is eliminated. Indeed, as reported in Ref. 4, laboratory results that were supposed to generate correlation peaks unequal in height, according to both theory and simulation, did not do so; they generated correlation peaks approximately equal in height.<sup>4</sup> The good laboratory results were attributed to the noise present in the laboratory system. This assumption was also supported by adding noise to an arrayed input in a computer-simulation experiment.

(2) One can eliminate the sidelobes by some processing method. This idea is the subject of Section 4.

#### 4. Space-Variant Thresholding

As indicated in Section 3, the PEC encounters difficulties when presented with several identical objects in a regular pattern. Although this is an infrequent occurrence, it is useful to modify the PEC in such a way that it performs well under these rare circum-

stances also. In this section we show that the difficulties can be alleviated by using a spatially varying threshold that processes the phase of the FT of the input function only if certain conditions are satisfied.

The difference between the SVTPEC and the regular PEC is that, whereas in the PEC the threshold is fixed at zero, in the SVTPEC it is spatially varied. The threshold used for the PEC can be represented in the complex domain by mapping every point onto the unit circle [Fig. 3(a)]. In the SVTPEC a threshold circle is defined for each point (spatial frequency) in the Fourier plane. A point on or outside the threshold circle is mapped, as before, onto the unit circle, but any point within the threshold circle is mapped to zero [Fig. 3(b)]. This procedure is repeated for every spatial frequency with a frequency-dependent threshold circle. The size of the circle usually decreases as the spatial frequency increases to take into account the decreasing amplitude with increasing spatial frequency of most objects. This ensures that low-amplitude information content present at the high spatial frequencies is not ignored, which maintains high-discrimination capabilities.

The space-variant-thresholding phase-extraction operation can be represented by the relation

$$N_i[Q(u, v)] = \begin{cases} \exp j \arg[Q(u, v)] & \text{if } |Q(u, v)|/Q_{\max} \geq t(u, v) \\ 0 & \text{otherwise} \end{cases}, \quad (11)$$

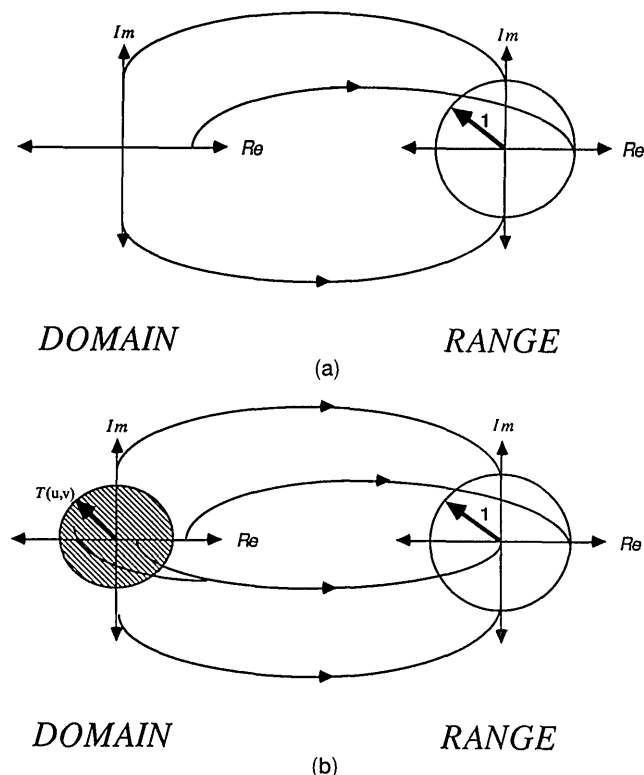


Fig. 3. Mapping performed by the nonlinearity: (a) the fixed (zero) threshold for the simple PEC and (b) the space-variant threshold for the SVTPEC.

where  $t(u, v)$  is a threshold function that should aid in achieving the following goals:

- (1) The true correlation peaks generated in the output (correlation) plane corresponding to the proper detection of objects in the input should be higher than any false peak.
- (2) The variance of the true peaks should be small.
- (3) The SVTPEC should be immune to noise.

Unfortunately, the above goals cannot be fully met simultaneously; nevertheless, good performance is possible, as is demonstrated in Subsection 4.C.

An input distribution composed of a regular array of  $N$  objects, each represented by a function  $a(x, y)/2$ , can be written in the form

$$q(x, y) = \sum_{n=0}^{N-1} \frac{a(x - nb - x_0, y)}{2}, \quad (12)$$

where  $x_0$  is the location of the center of the first object. This function is Fourier transformed to

$$\begin{aligned} Q(u, v) &= \left| \frac{A(u, v)}{2} \right| \exp j\varphi(u, v) \\ &\times \exp(-j2\pi u x_0) \sum_{n=0}^{N-1} \exp(-j2\pi u n b) \\ &= |A(u, v)| \exp[j\varphi(u, v)] R(u) \frac{\sin(\pi u b N)}{2 \sin(\pi u b)}, \end{aligned} \quad (13)$$

where we define

$$A(u, v) \equiv |A(u, v)| \exp j\varphi(u, v) = \mathcal{F}[a(x, y)], \quad (14)$$

$$R(u) = \exp(-j2\pi u x_0) \exp[-j\pi u(N-1)b]. \quad (15)$$

To detect the input patterns  $a(x, y)$ , we define a matched filter function

$$p(x, y) = a(-x, -y), \quad (16)$$

where we assume real input functions for simplicity.

Choosing a spatially varying threshold by the relation (as first suggested in Ref. 4)

$$t(u, v) = \mu \frac{|A(u, v)|}{A_{\max}}, \quad 0 < \mu < 1, \quad \mu \in \text{Re}, \quad (17)$$

we obtain an output that is totally independent of the specific object under consideration, as is shown in Subsection 4.C. Here,  $A_{\max} = \max[|A(u, v)|]$ . This choice of  $t(u, v)$  guarantees that the envelope of  $|\mathcal{F}[a(x, y)]|$ , to which the filter is matched, is followed, and it guarantees that low-amplitude information of the subsidiary maxima [caused by the sidelobes of  $\sin(\pi u b N)/2 \sin(\pi u b)$  in Eq. (13)], which may degrade system performance, is not amplified. Nevertheless, the phase information in the higher spatial frequencies is still used for the recognition process owing to

the decreasing amplitude of  $t(u, v)$ , which is proportional to the reduction in amplitude of  $A(u, v)$ .

#### A. Similarity of Phase-Extraction Correlator and Offsprings of Binary Joint Transform Correlator

It should be noted that the entire analysis presented in Section 3 and the analysis in this section may be adapted and applied directly to the binarization of the JTC spectrum<sup>10</sup> (severe nonlinearity) by the use of an appropriate threshold function.<sup>11</sup> Following the notation of Javidi *et al.*,<sup>10</sup> let the input and reference functions,  $s(x - x_0, y)$  and  $r(x + x_0, y)$ , respectively, both be displayed on an input transparency. Denoting their FT's by  $S(u, v)$  and  $R(u, v)$ , we obtain at the FT plane, after performing the FT of the input transparency, an intensity distribution

$$\begin{aligned} I(u, v) &= |S(u, v)|^2 + |R(u, v)|^2 + 2|S(u, v)R(u, v)| \\ &\times \cos[\phi_R(u, v) - \phi_S(u, v) + 2\pi u x_0], \end{aligned} \quad (18)$$

where  $(u, v)$  are the spatial frequencies,  $\phi_R(u, v) = \arg[R(u, v)]$ , and  $\phi_S(u, v) = \arg[S(u, v)]$ . Defining  $H(u, v)$  as the result of a bipolar binarization process that operates on  $I(u, v)$ ,

$$H(u, v) = \begin{cases} 1 & \text{if } I(u, v) \geq t(u, v) \\ -1 & \text{otherwise} \end{cases}, \quad (19)$$

where the spatially varying threshold function  $t(u, v)$  (as opposed to the constant threshold function used by Javidi *et al.*<sup>10</sup>) is chosen as

$$t(u, v) = |R(u, v)|^2 + |S(u, v)|^2, \quad (20)$$

and performing the FT of  $H(u, v)$ , yields the correlation plane that is functionally identical to the correlation plane generated by the PEC (except for the carrier frequency, which is also introduced actually in the optical implementation of the PEC<sup>4</sup>). That is, the FT of  $H(u, v)$ , which yields the binary joint transform correlation plane, is totally independent of the Fourier amplitude (intensity) of  $S(u, v)$  and  $R(u, v)$ , depending only on its Fourier phase like the PEC. Employing this specific threshold function [Eq. (20)] in the binary JTC, we obtain a response that is functionally identical to phase-only correlation (filter and input). This is different than other thresholding procedures used previously.<sup>11,12</sup>

At this point it should also be emphasized that the space-variant thresholding employed by the SVTPEC, as given by Eq. (17), is totally different than the adaptive threshold employed by Hahn and Flannery<sup>11</sup> for the binary JTC. The adaptive threshold was employed basically to obtain clean periodic fringes in the FT plane (see Fig. 2 of Ref. 11), similar to the function of the PEC [or its equivalent binary JTC implementation that uses an adaptive threshold obtained by Eq. (20)]. However, in the SVTPEC, rather than enhancing the information contained in the interference fringes, we tend to ignore some of it because this information is unimportant and may lead to poor results, as is explained in Subsection 4.B.

Thus, although the threshold obtained by Eq. (20) in the binary JTC may also be termed an adaptive threshold, as it is in Ref. 11, it should not be confused with the type of thresholding employed by the SVT-PEC, obtained by Eq. (17), which leads to different results.

## B. Discussion

At this point it is useful to understand the fundamental underlying reason for the failure of the PEC in the case of regular-array input configurations. In Refs. 7 and 8 it was shown that a signal cannot be restored from its Fourier phase alone if the original signal  $q(x)$  can be represented as

$$q(x) = a(x) * b(x), \quad (21)$$

where, for clarity we use one-dimensional functions and  $b(x)$  is a zero phase sequence [the FT of  $b(x)$  being a real function].

The input obtained by Eq. (12) is obviously such a case, as is evident from Eq. (13), since  $\sin(\pi ubN)/\sin(\pi ub)$ , which is the FT of the displacement sequence, if properly centered, is always a real quantity. Moreover, the displacement information is largely coded into the amplitude distribution, leaving the phase information almost transparent to it. Therefore the phase distribution alone does not contain adequate information to restore the complete signal or to perform correlations. The SVTPEC is designed to perform detection and discrimination with a high reliability by selectively processing the phase based on the input's spectral amplitude distribution. Thus the additional information present, although not actually manipulated, is used as a means to process the phase more appropriately. Figure 4 shows the operation of the SVTPEC.

Assume that the input is obtained by Eq. (12) with  $N = 4$  and  $x_0 = -1.5b$ . Without loss of generality, let  $A(u, v)$  be obtained as shown in Fig. 4(b). The sum of linear phases,  $\sin(8\pi ux_0)/2 \sin(2\pi ux_0)$ , is shown in Fig. 4(a). Hence  $Q(u, v)$  is obtained by the product of Figs. 4(a) and 4(b) and is shown in Fig. 4(c). Defining  $A_{\max}$  in a similar manner to  $Q_{\max}$ , we obtain Fig. 4(d) as the result of applying the simple nonlinearity of Eq. (1), to  $Q(u, v)$ . If we apply the space-variant nonlinearity of Eq. (11) with  $t(u, v)$  of Eq. (17) and  $\mu = 0.25$  to  $Q(u, v)$  we obtain Fig. 4(e). The above-mentioned value for  $\mu$  was chosen since it is the maximum value that will still eliminate the low-amplitude subsidiary maxima in the four-identical-object input case. Examination of Fig. 4(d) reveals that the PEC fails in the regular arrayed input because the low-amplitude sidelobes are turned into a periodic high-frequency grid that multiplies the Fourier phase of the input objects. This high-frequency grid is not present in Fig. 4(e), in which the phase is purified, retaining only the phase corresponding to the main lobes.

Dwelling on this point further, we note that the high-frequency grid, produced by the PEC, can be shown to correspond to a separation of  $(N - 1)b$

between correlation spots in the correlation plane. This grid becomes more dominant as the number of objects is increased, since the number of sidelobes increases as well. In this case, Fig. 4(c) would become a train of delta functions that is multiplied by an envelope function [Fig. 4(a)]. This is shown in Fig. 5(a), but for the envelope function, which is suppressed for convenience. Application of simple nonlinearity to Fig. 5(a) yields Fig. 5(b), in which the dominance of the high-frequency grid is clear. This is in contrast to the operation of the SVTPEC, which, by preserving solely the main lobes, produces a signal that is free of the high-frequency artifact, as is shown in Fig. 5(c). The resulting frequency of the grid in Fig. 5(c) can easily be shown to correspond to the correct separation  $b$  between the correlation peaks in the correlation plane. Consequently, the close resemblance that Fig. 5(c) bears to Fig. 5(a) (which retains all displacement information) is expected, and the distortion put forward by the simple nonlinearity (the simple PEC) is also clear. Hence the good performance of the SVTPEC that is shown in simulations in Section 5 and that is derived analytically in Subsection 4.C, is to be expected.

However, this raises a serious question. We claim that we are able to manipulate the phase in some manner and to generate true correlation peaks even when  $b(x)$  of Eq. (21) is a zero phase signal. This seems to contradict results obtained by Hayes *et al.*<sup>7</sup> and others. However, this is not so since after application of the SVTPEC we incorporate some amplitude variation as well and do not just extract the phase from  $b(x)$ . Hence we have not only the limited phase information of  $b(x)$  [and  $a(x)$ ], we also multiply by an appropriate modulating term.

## C. Space-Variant-Threshold Phase-Extraction Correlator: Analytical Derivation of Correlation

A block diagram of an SVTPEC that uses the threshold function  $t(u, v)$  of Eq. (17) is shown in Fig. 6. Setting  $\mu$  in Eq. (17) to a value that guarantees that the largest subsidiary maximum in Eq. (13) is eliminated, which preserves only the spectral regions corresponding to the main lobes of  $[\sin(\pi ubN)/2 \sin(\pi ub)]$  [where  $\sin(\pi ubN)/2 \sin(\pi ub) \geq \mu$ ], leads to the complex amplitude distribution

$$c(u, v) = R(u) \left[ \sum_{n=-\infty, n \text{ even}}^{\infty} \text{rect} \left( \frac{u - \frac{n}{b}}{2u_t} \right) + \sum_{n=-\infty, n \text{ odd}}^{\infty} \text{rect} \left( \frac{u - \frac{n}{b}}{2u_t} \right) (-1)^{N+1} \right] \quad (22)$$

just before the IFT is performed. The parameter  $2u_t$  is a constant and is the width of the samples in the frequency plane, which depends on the spatially varying threshold  $t(u, v)$ . Note that, as mentioned above, the phase is sampled at regular intervals, and the high spatial frequencies contribute to the output

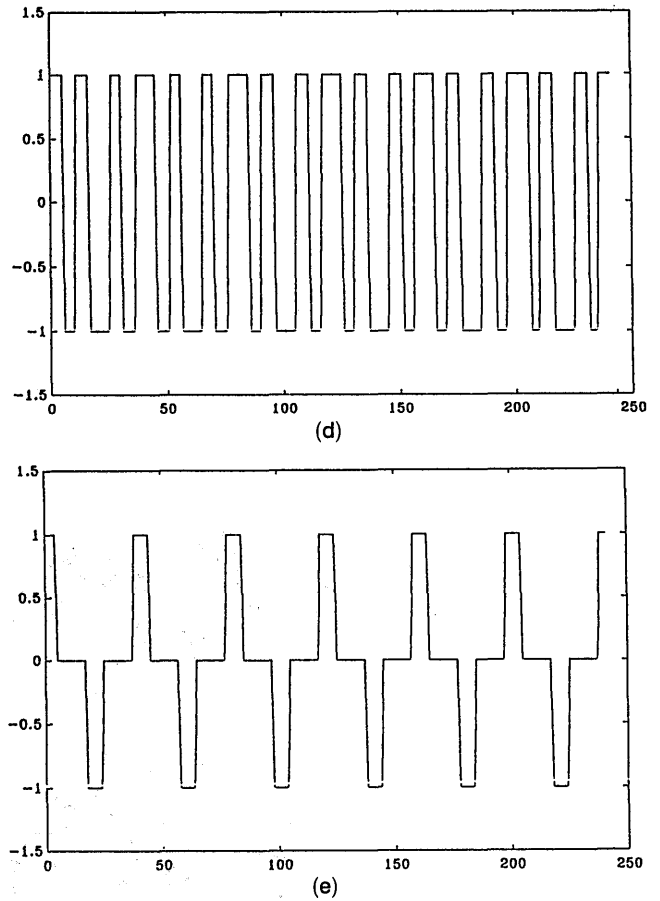
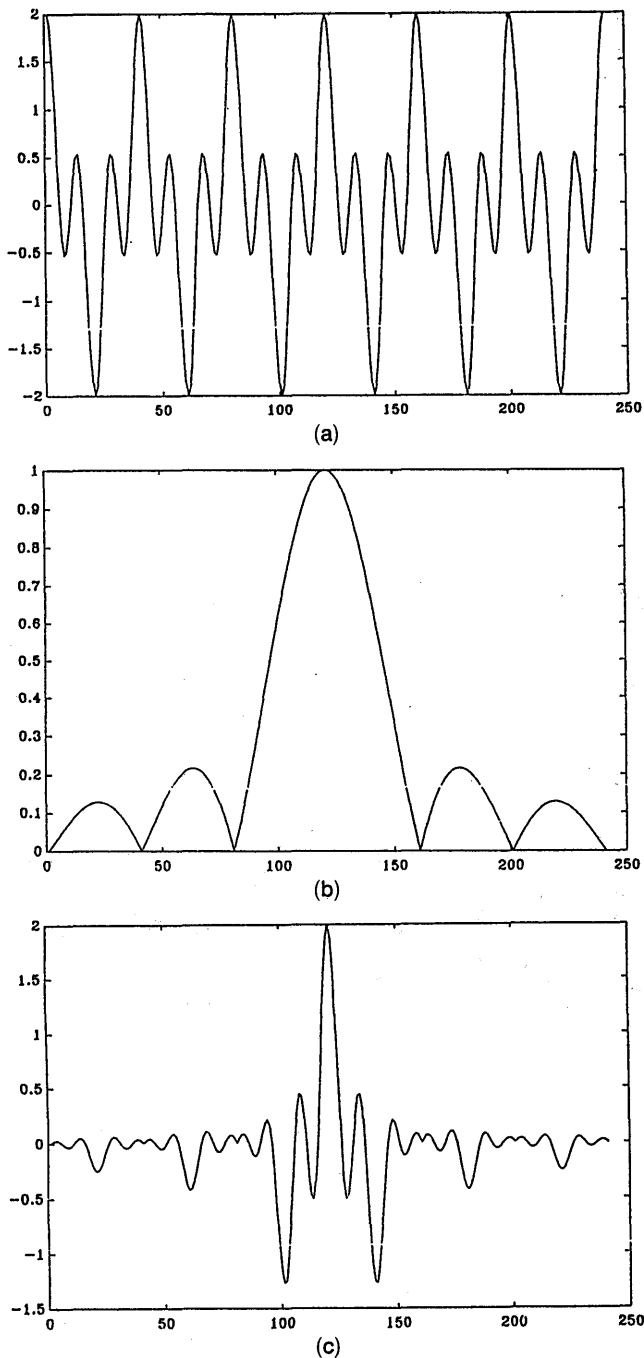


Fig. 4. (a) Distribution of  $\sin(8\pi ux_0)/2 \sin(2\pi ux_0)$ . (b) Amplitude distribution of a typical spectrum of an object. (c) Product of (a) and (b) above obtained by Eq. (13) with  $x_0 = -1.5c$  and  $N = 4$ . (d) Result of the simple nonlinearity, obtained by Eq. (1) and with  $l = 0$ , applied to (c) above. (e) Result of the selective nonlinearity, obtained by Eq. (11), applied to (c) above. Note that the horizontal axis is the frequency plane axis.

correlation function. It should also be noted that the wider the samples, the more phase information is processed.

The final correlator output is obtained by performing the IFT on Eq. (22):

$$C(x, y) = \mathcal{F}^{-1}c(u, v) = B \operatorname{sinc}[2u_t(x - x_c)] \times \left[ \sum_{n \text{ even}}^{\infty} \delta(x - nb - x_c, y) + \sum_{n \text{ odd}}^{\infty} (-1)^{N+1} \delta(x - nb - x_c, y) \right], \quad (23)$$

where  $x_c = x_0 + [(N - 1)b/2]$  (the center of the shifted input) and  $B$  is some constant depending on  $u_t$  and  $b$ .

The proper choice of the parameters  $\mu$  and  $u_t$  is closely interrelated and needs to be determined. Equating the normalized amplitude of Eq. (13) (the spectral distribution of the input) to the amplitude of Eq. (17) (the spectral distribution of the threshold) yields

$$\frac{\sin(\pi ubN)}{\sin(\pi ub)} |A(u, v)| = \mu |A(u, v)| N. \quad (24)$$

Since  $|\sin(\pi ubN)/\sin(\pi ub)|$  is periodic, we may con-

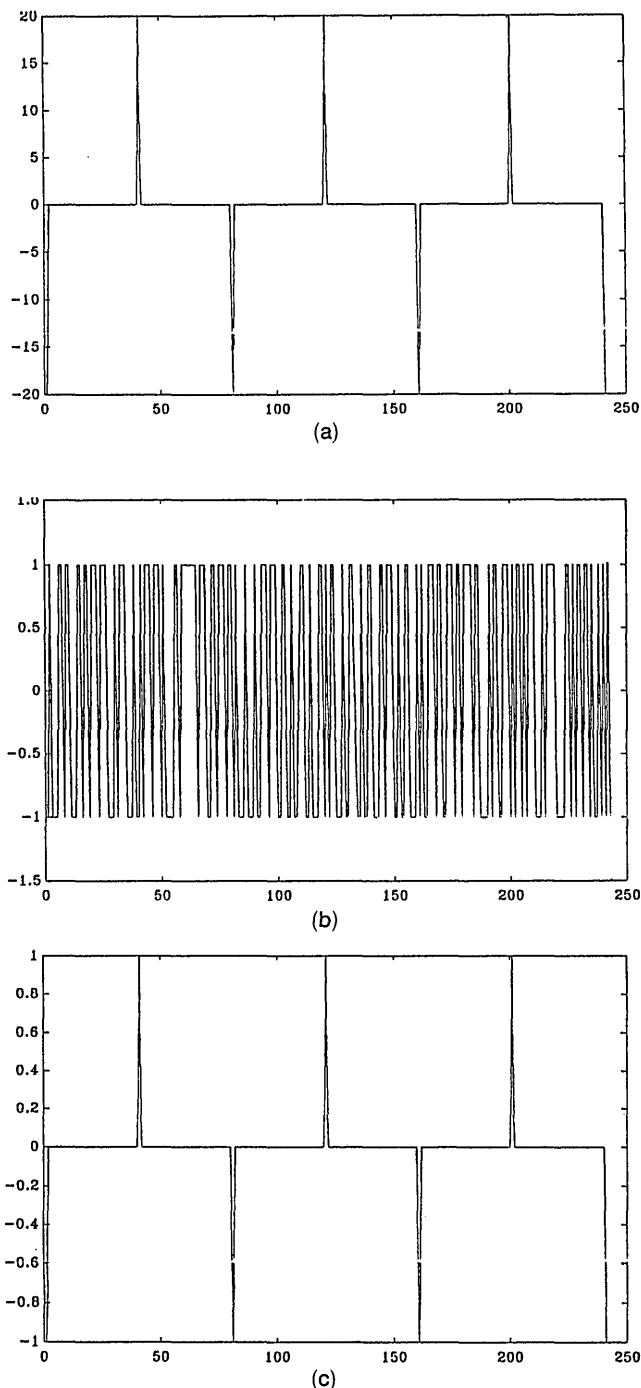


Fig. 5. (a) Distribution of  $\sin(80\pi ux_0)/2 \sin(2\pi ux_0)$ . (b) Result of the simple nonlinearity, obtained by Eq. (1), applied to (a) above. (c) Result of the selective nonlinearity, obtained by Eq. (11), applied to (a) above.

fine our analysis to  $0 < \pi ub < \pi$  and assume that this condition is satisfied periodically, with period  $\pi$ . To attain this first goal, we require

$$0 < \pi ubN < \pi \quad (25)$$

to be between the maximum of  $|\sin(\pi ubN)/\sin(\pi ub)|$  at  $u = 0$  and its first zero. This can also be written as

$$0 < ub < \frac{1}{N}. \quad (26)$$

This constraint guarantees that  $u$  is in the region in which Eq. (24) can be satisfied (between the principal maxima and the first zero), but it does not guarantee that the sidelobes are reduced. For most practical cases, however,

$$ub \ll \frac{1}{N}, \quad (27)$$

since in principle we want a large  $\mu$  for reasons that become apparent from the analysis below. This automatically takes care of the sidelobe reduction.

Assuming that inequality (27) is satisfied, we may approximate

$$\sin(\pi ubN) \approx \left[ \pi ubN - \frac{(\pi ubN)^3}{6} \right], \quad (28)$$

$$\sin(\pi ub) \approx (\pi ub). \quad (29)$$

In relation (28) we take two terms into account since  $N\pi ub$  is not as small as  $\pi ub$  in relation (29), in which one term suffices for the series expansion. Substitution of relations (28) and (29) into Eq. (24) yields a quadratic equation whose solution is (since  $u \in \text{Re}^+$ )

$$u_t = \pm \frac{[6(1 - \mu)]^{1/2}}{N\pi b}, \quad (30)$$

where  $u_t$  can now be interpreted as the spatial frequency below which the variable threshold will process the phase of  $Q(u, v)$ . In other words, for  $0 < u < u_t$  and  $1/b - u_t < u < 1/b$  the phase of  $Q(u, v)$  is processed. (Remember, this analysis is periodic with period  $\pi$  on the quantity  $\pi ub$ .)

Thus the thresholded signal of Eq. (22), which may also be written as

$$c(u, v) = \left\{ \sum_{-\infty}^{\infty} \left[ \delta\left(2u - \frac{2n}{b}\right) + (-1)^{N+1} \delta\left(u - \frac{2n+1}{b}\right) \right] * \text{rect}\left(\frac{u}{2u_t}\right) \right\} R(u), \quad (31)$$

yields the correlation output by performing the IFT on Eq. (31), which is

$$C(x, y) = (2\pi u_t b) \text{sinc}[2u_t(x - x_c)] \times \sum_{n=-\infty}^{\infty} \delta\left(x - x_c - \frac{bn}{2}, y\right) [1 + (-1)^{n+N+1}]. \quad (32)$$

Thus  $\delta$  functions are obtained at the correct positions of the objects, but these are multiplied by an envelope of a sinc function. Thus  $u_t$  should be adequately small to make the sinc function barely change over the interval of interest  $[x_o < x < x_o + (N - 1)b]$ .

Determining  $u_t$  solely by this consideration may lead to unfavorable results since  $u_t$  sets a unique

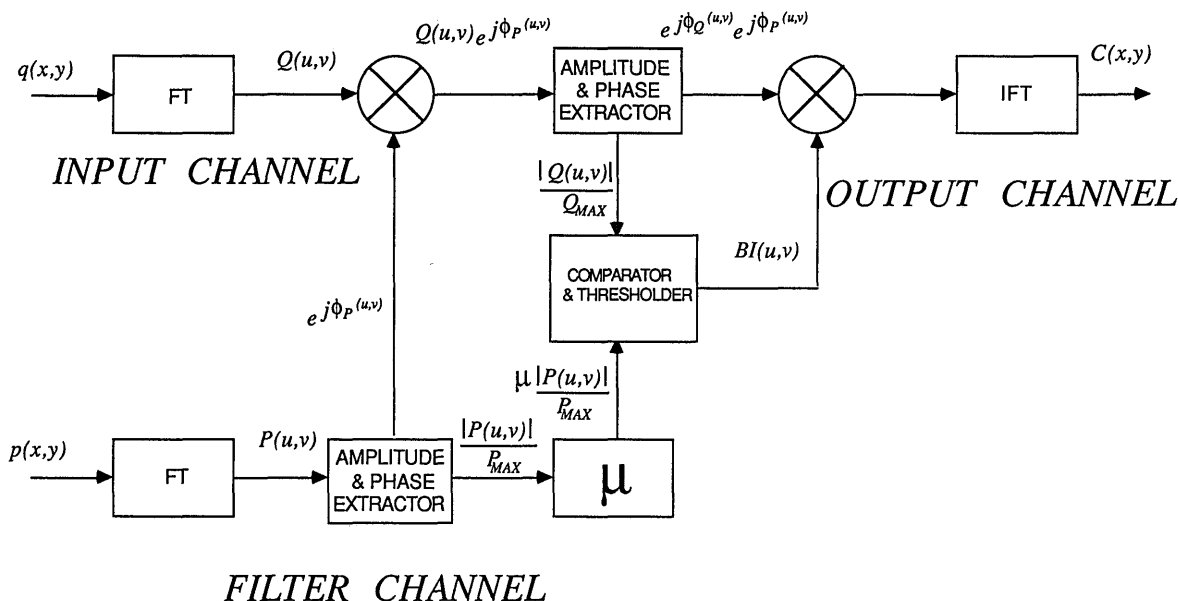


Fig. 6. Block diagram of the SVTPEC, in which  $BI(u, v)$  is the binary output of the COMPARATOR & THRESHOLDER. It may assume the following values:

$$BI(u, v) = \begin{cases} 1 & \text{if } |Q(u, v)|/Q_{\max} \geq \mu[|P(u, v)|/P_{\max}] \\ 0 & \text{otherwise} \end{cases}$$

value on the threshold parameter. Inverting Eq. (30), we have

$$\mu = 1 - \frac{(N\pi b u_t)^2}{6}. \quad (33)$$

Decreasing  $u_t$  (making the rectangular pulses in the frequency domain thinner) implies, effectively, increasing the threshold factor  $\mu$ . Theoretically, this would not pose a problem. Practically, however, if the frequency plane contains noise, and if the threshold is too high, some principal maxima in the frequency plane generated by the sum of linear phases might be missed, thus corrupting the location information. Hence some compromise has to be made between immunity to noise (the third goal) and the variance of the output delta peaks (the second goal) in the choice of the threshold. The ratio between the minimal and maximal peaks for an input described by Eq. (12) is obtained by

$$\frac{\text{minimum true peak}}{\text{maximum true peak}} = \frac{u_t \operatorname{sinc}(2u_t x)_{@x=Nb/2}}{u_t \operatorname{sinc}(2u_t x)_{@x=b/2}} = \frac{\sin\{[6(1-\mu)]^{1/2}\}}{N \sin\left\{\frac{[6(1-\mu)]^{1/2}}{N}\right\}}. \quad (34)$$

As the threshold factor  $\mu$  approaches unity, the ratio approaches unity, implying zero variance of the output correlation peaks. Numerical investigations demonstrated a maximum ratio of the deltas at the centers of the objects in the output correlation plane of 0.77 to 0.95 as  $\mu$  was changed from 0.75 to 0.95.

These ratios were almost completely independent of the number of objects present. Hence for a low-noise background the SVTPEC performs equally well for single- or multiple-object detection.

The computer experiments presented in Section 5 support our conclusion that the problem of peak position dependence is dramatically reduced. It is also demonstrated that, for objects arranged randomly in the input plane, the performance of the SVTPEC is not substantially inferior to the regular PEC; thus the SVTPEC may be employed for any input configuration and is preferential when periodic inputs can be expected. The remaining concern about the SVTPEC is the reduction in discrimination owing to some disposition of (phase) information. As shown in Section 5, this feature too is barely impaired by the SVTPEC and in some cases is even improved.

## 5. Simulation Experiments

For the simulation experiments we set the threshold factor to  $\mu = 0.25$  [see Eqs. (11) and (17)]. This value of  $\mu$  is the lowest permitted value that still ensures the elimination of the sidelobes generated in the case of four equally spaced objects centered on a line.

Letters of the size  $10 \times 10$  pixels were created and placed in an input plane of size  $128 \times 128$  pixels. The FT of the input was taken with an FFT. The POMF was also stored in  $128 \times 128$  pixels. The output correlation was obtained by taking the FT of the product of the POMF, which was multiplied by the result of the nonlinearity applied to the input. The input distributions for some experiments are shown in Fig. 7. The correlation outputs shown in

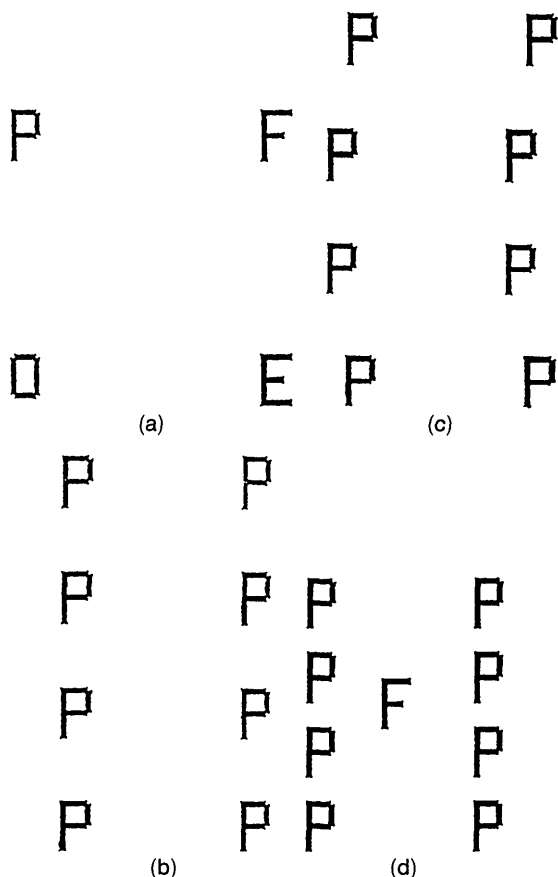


Fig. 7. Four input distributions used in the simulations.

Fig. 8 were obtained by the simple PEC; they show generally good performance but demonstrate the problem of periodic input. In Fig. 9 we have the output of the SVTPEC for the inputs of Fig. 7. Various observations can be made with reference to Fig. 9:

(1) The discrimination provided by the SVTPEC is comparable with that provided by the simple PEC, as expected.

(2) The widths of the peaks, generated by the SVTPEC, are no different from those of the simple

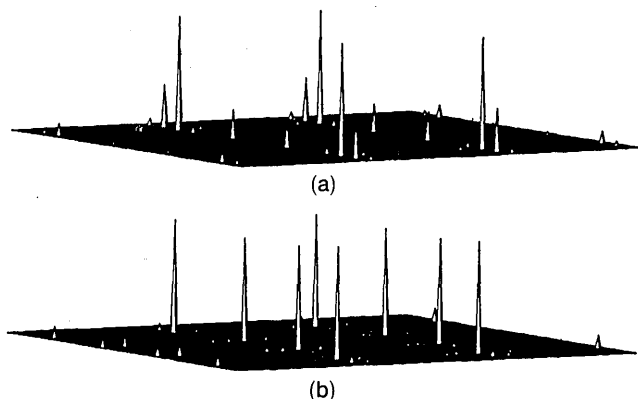


Fig. 8. Correlation plane of the PEC, with a POMF matched to the letter P: (a) Fig. 7(b) as the input and (b) Fig. 7(c) as the input.

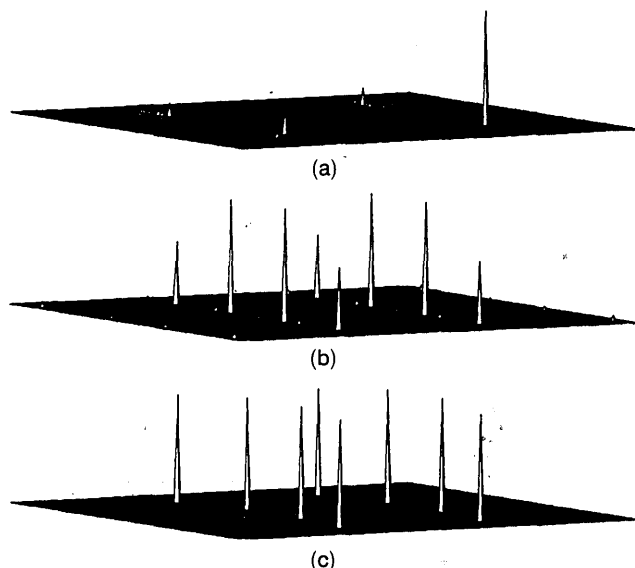


Fig. 9. Output correlation planes of the SVTPEC when Figs. 7(a)–(c) are the inputs: (a) Fig. 7(a) as the input, (b) Fig. 7(b) as the input, and (c) Fig. 7(c) as the input. (in all cases the filter is matched to the letter P).

PEC. Hence it may be stated that the inverse-filter-like performance is still achieved with the SVTPEC. This is in accordance with the theory developed for the SVTPEC for the case of equally spaced objects, in which we obtained delta functions at the true locations of the centers of the objects with no spurious peaks [see Eq. (32)].

(3) Although the concept of the specific type of the space-variant threshold originated from an equal-spacing setup, in which strong main lobes are present, the SVTPEC performed equally well in the pseudo-random-spacing setup [Fig. 9(c)].

Consider the input in Fig. 7(d). Clearly the spectrum of the input will be composed primarily of the spectrum of the letter P (as there are eight P's), and hence when extracting the phase of the spectrum, one would expect that the phase of F is buried in the heavier weight of the eight P's. Indeed, in Fig. 10(a) we see that the simple PEC is not able to provide sufficient discrimination against the letter F (actually not at all) when the filter function is phase matched to P. However, the SVTPEC, which acts as a selective phase extractor, is able to provide good discrimination against the letter F [see Fig. 10(b)]. This phenomenon is not yet well understood; compare the good discrimination provided by the PEC when the filter is matched to F, shown in Fig. 11. However, since the SVTPEC contains more information than the PEC, as the phase processing is based on some spectral amplitude variation information that is unavailable to the PEC, it is expected to yield similar or better discrimination than the PEC, despite the partial disposition of phase. Also, the operation of the SVTPEC (selective phase extractor) on the spectral input distribution is conceptually similar to that of a phase-only filter multiplied by a binary unipolar

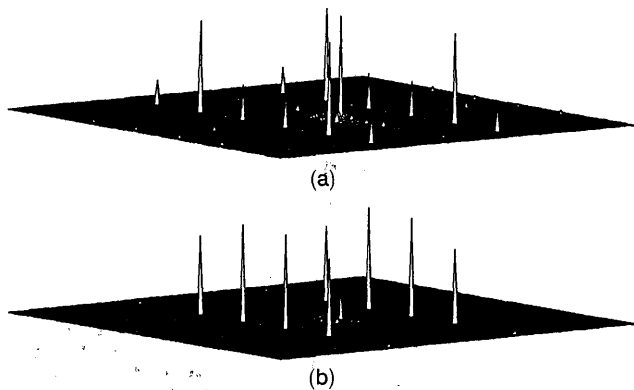


Fig. 10. Output correlation distribution when Fig. 7(d) is the input for (a) the simple PEC and (b) the SVTPEC.

amplitude filter. These types of combined phase-amplitude filters are known to obtain better discrimination than their phased-only filters counterparts.<sup>13</sup> Hence the SVTPEC, whose nonlinear operation is similar conceptually to the combination of the above filters, is expected to obtain better discrimination and selectivity than the simple PEC, as we observed in the case of the filter matched to P, which is shown in Fig. 10.

#### 6. Optical Implementation of Space-Variant-Threshold Phase-Extraction Correlator

To keep this section brief, we refer the reader to our earlier research<sup>1,4</sup> concerning the simple PEC and its optical implementation. The SVTPEC can be optically implemented by the addition of a third 0 state (in addition to the +1 and -1 states employed in our earlier research) in order to record the frequency mask. This may be performed with commercially available magneto-optic spatial light modulators. In addition to the two stable bipolar states used earlier,<sup>4</sup> one may use the mixed magnetization state for the zero modulation required.<sup>14</sup> Empirically, when the input's amplitude distribution is not less than the threshold, the phase is processed, as described previously (assigned either a +1 or -1 state); otherwise it is ignored and assigned the 0 state. Unfortunately, however, because of the degradation of our Semetex magneto-optic spatial light modulator (~30% dead lines), we were not able to employ this option. Instead, we had to use the less-efficient unipolar implementation of the PEC<sup>1</sup> by recording the frequency mask on a transparency in the following manner: (1) The 1 state is assigned as 1, as in the bipolar case. (2) The 0 state is assigned to the  $\frac{1}{2}$  state. (3) The -1 state is assigned to the 0 state.

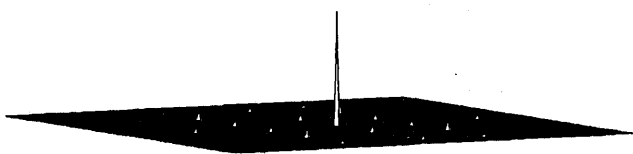


Fig. 11. Simulated output of the PEC with a POMF matched to the letter F and with the input obtained by Fig. 7(d).

The experiment proceeded as follows: The FT of the input and filter functions was performed optically so that both the phase of the FT of the filter and input functions and the amplitude distribution of the FT of the filter and input functions were recorded (the latter was not needed in the optical implementation of the simple PEC). Thresholding was then performed electronically by computer, and the result was recorded on a transparency according to the unipolar implementation mentioned above. Finally, the IFT was performed (optically) to obtain the correlation plane.

At this point we recall that the addition of low-amplitude noise to the input destroys the low-amplitude subsidiary sidelobes created by the sum of linear phases. Since in the laboratory there is substantial noise,<sup>4</sup> the problematic features of the PEC were never observable in laboratory experiments. Therefore it is not expected that the results from the optical implementation of the SVTPEC would be substantially different from those obtained by the PEC. This was indeed confirmed experimentally. Also the discrimination provided by the SVTPEC was similar to that provided by the PEC. We show just one of the outputs obtained experimentally by the above-mentioned method in order to keep our scope within reasonable bounds. With the input shown in Fig. 7(a) and a filter matched to P, we obtained by the optical SVTPEC the first diffraction order of the output correlation plane, which is shown in Fig. 12. Both the discrimination provided by the SVTPEC and the correlation-peak sharpness are similar to the results obtained by the PEC (Fig. 13). In Ref. 4 these were shown to be better than could be obtained by similar linear correlators.<sup>4</sup> This demonstrates the superiority of the PEC and its offspring over the conventional linear correlators for optical detection

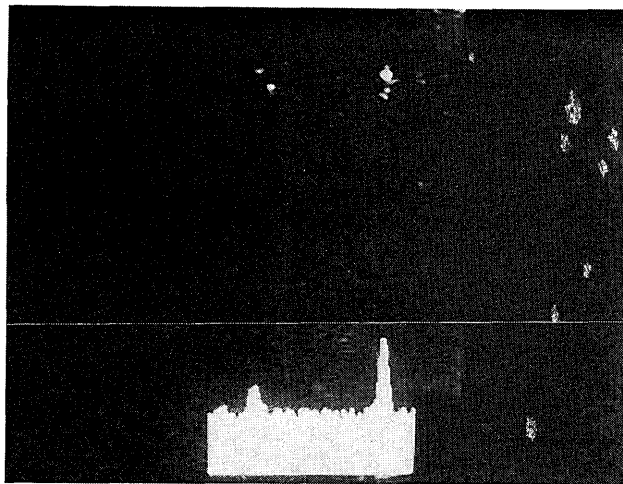
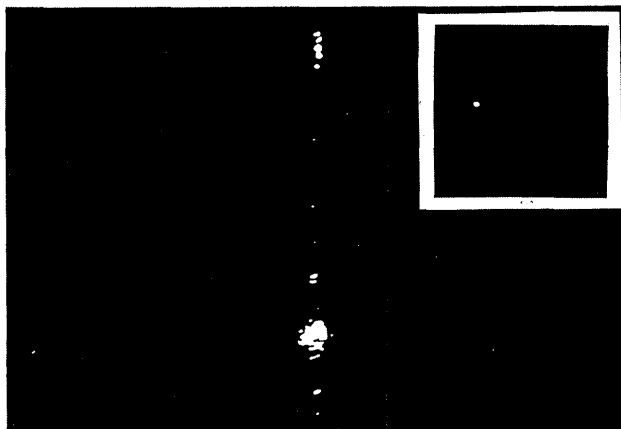
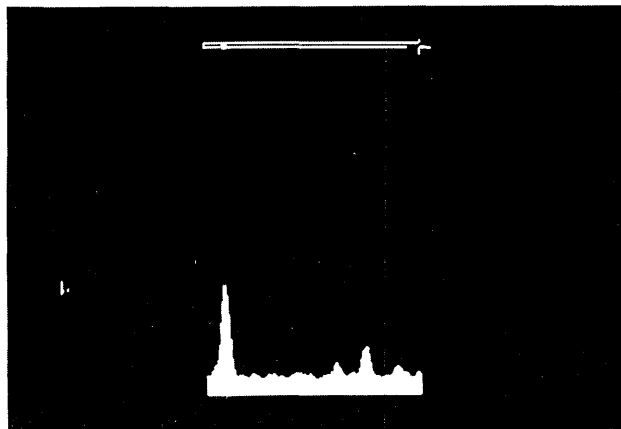


Fig. 12. First diffraction order of the output correlation plane generated by the SVTPEC when the input function  $q(x, y)$  is obtained by Fig. 7(a) and the filter is a POMF matched to the letter P. The transverse cross section of the correlation peaks corresponding to the letters P and F is also shown. Note that the transversal cross sections' physical dimensions are equal to the transversal dimensions of the input shown in Fig. 7(a).



(a)



(b)

Fig. 13. (a) Output correlation plane (marked by window) of the PEC with the input shown in Fig. 7(a). (b) Transverse cross section of the correlation plane corresponding to the letters P and F in Fig. 7(a).

and recognition purposes, except, possibly, for the lack of strict shift invariance. We also note that the similarity between Figs. 12 and 13, except for the level of noise present in the figures (which is irrelevant to discrimination and peak sharpness), is in accordance with our expectations as presented in Sections 4 and 5.

## 7. Conclusions

We have demonstrated and analyzed the practical feasibility of achieving a phase-extraction pattern-recognition system. We have also examined an improved space-variant phase-extraction pattern-recognition system that may be a practical solution to the problems of the former simple PEC. Simulation, optical results, and analytical results revealed that the space-variant-threshold PEC still maintained the discrimination and narrow correlation peaks observed with the simple PEC. The price, however, is a lower optical efficiency since the phase distribution of those spatial frequencies that are not processed is ignored and does not contribute to the output correlation function. Finally, it has been shown that the SVTPEC performs well for either single- or multiple-

object inputs located in the input in either an arranged or a random pattern.

This work was performed within the Technion Advanced Opto-Electronics Center, which is supported by the American Technion Society, New York.

## Appendix A: Derivation of Mean and Variance

Define  $E[f_x(x, y)]$  as the statistical expectation value of  $f(x, y)$  with respect to  $x$ ; i.e.,

$$E_x[f(x, y)] = \int_{-\infty}^{\infty} f(x, y)\rho(x)dx, \quad (\text{A1})$$

where  $\rho(x)$  denotes the probability density function of  $x$ . Let  $x_i$  be an independent and identically distributed random variable, with its probability density distributed as

$$\rho(x_i) = \begin{cases} \frac{1}{2a} & \text{for } |x_i| < a \\ 0 & \text{otherwise} \end{cases}. \quad (\text{A2})$$

We have from the definition of  $D(u)$  in Eq. (8) that

$$E_{x_i}[D(u)] = \sum_{i=1}^N \sum_{l=1, l \neq i}^N E[\exp j2\pi u(x_i - x_l)]. \quad (\text{A3})$$

Since  $x_i$  and  $x_l$  are for  $i \neq l$  independent random variables, from statistical analysis we have

$$\begin{aligned} & E_{x_i}[\exp(j2\pi ux_i)\exp(-j2\pi ux_l)] \\ &= \{E[\exp(j2\pi ux_i)]\}^2 = \left[ \int_{-a}^a \frac{\exp(j2\pi ux_l)}{2a} dx_l \right]^2, \end{aligned} \quad (\text{A4})$$

since  $x_i$  and  $x_l$  are identically distributed as well, with their distribution obtained by Eq. (A2). Hence

$$E_{x_i}[D(u)] = N(N-1)\text{sinc}^2(2ua). \quad (\text{A5})$$

We define the random process

$$v(u) = \mathcal{F}[V(x)] = \frac{1}{[N + D(u)]^{1/2}} \quad (\text{A6})$$

and wish to prove that  $V(x)$  is a spatially narrow-band function with low variance as compared with its mean. To simplify notation, we omit the index  $x_i$  in the following discussion. By definition, we have

$$E[V(x)] = E\{\mathcal{F}^{-1}[v(u)]\} = E\left\{ \int_{-\infty}^{\infty} \frac{\exp j2\pi ux}{[N + D(u)]^{1/2}} du \right\}. \quad (\text{A7})$$

We know that the FT of an input, in the region of the zero spatial frequency, obtains the average (dc) term of the input. Hence we separate this region from the rest in Eq. (A7) and subsequent formulas. Also, remember that we have a finite aperture in the spatial

frequency domain and that its size is  $A$ . Thus we may write

$$E[V(x)] \approx E\left\{\frac{1}{[N + D(0)]^{1/2}} + \int_{-A/2, u \neq 0}^{A/2} \frac{\exp j2\pi ux}{[N + D(u)]^{1/2}} du\right\}, \quad (\text{A8})$$

which, after some algebraic manipulation and expansion in a series, leads to

$$\frac{1}{N} + E\left(\int_{-A/2, u \neq 0}^{A/2} \frac{\exp j2\pi ux}{\sqrt{N}} \times \left\{\sum_{p=1}^{\infty} 1 + \frac{(-1)^p \alpha_p}{p!} \left[\frac{D(u)}{N}\right]^p du\right\}\right), \quad (\text{A9})$$

where  $\alpha_p$  is obtained by

$$\alpha_p = (1/2)(3/2) \cdots (1/2 + p - 1). \quad (\text{A10})$$

Since the mean of  $D(u)$  is zero except in the neighborhood of  $u \approx 0$ , where it is  $N(N-1)$  [see Eq. (A5)], if the input aperture size ( $2a$ ) is large, we may approximate the above equation by keeping only the first term in the series expansion:

$$E[V(x)] \approx \frac{1}{N} + A \frac{\text{sinc}(Ax)}{\sqrt{N}}. \quad (\text{A11})$$

Note that, for a large aperture in the Fourier domain ( $A$ ), this expectation value is highly concentrated:

$$E[V(x)] \rightarrow \frac{\delta(x)}{\sqrt{N}}. \quad (\text{A12})$$

The second moment of  $V(x)$  is obtained by

$$\begin{aligned} E[V^2(x)] &= E\{\mathcal{F}^{-1}[v(u) * v(u)]\} \\ &= E\left[\int_{-A/2}^{A/2} \exp j2\pi ux \int_{-A/2}^{A/2} v(u')v(u-u') du' du\right]. \end{aligned} \quad (\text{A13})$$

Analogous to our treatment above, we separate the  $u \approx 0$  region and obtain

$$\begin{aligned} E[V^2(x)] &= E\left\{\int_{-A/2}^{A/2} v^2(u') du' + \int_{-A/2, u \neq 0}^{A/2} \exp j2\pi ux \right. \\ &\quad \left. \times \int_{-A/2}^{A/2} \frac{1}{[N + D(u')]^{1/2}[N + D(u-u')]^{1/2}} du' du\right\} \end{aligned} \quad (\text{A14})$$

since  $D(u)$  is a symmetric function. After separating the double integral we may again use a series expansion:

$$\begin{aligned} E[V^2(x)] &\approx \frac{A}{N} \left\{1 + \sum_{p=2}^{\infty} \frac{(-1)^p b_p}{p!} E\left[\frac{D(u')^p}{N}\right]\right\} \\ &\quad + E\left(\int_{-A/2}^{A/2} \frac{1}{\sqrt{N}} \left\{1 + \sum_{p=1}^{\infty} \frac{(-1)^p \alpha_p}{p!} \left[\frac{D(u')}{N}\right]^p\right\} \right. \\ &\quad \left. \times \exp(j2\pi u'x) du'\right)^2, \end{aligned} \quad (\text{A15})$$

which, to first-order approximation, can be written in the simple form

$$E[V^2(x)] \approx \frac{A}{N} + \frac{[A \text{sinc}(Ax)]^2}{N}, \quad (\text{A16})$$

where

$$b_p = (1)(2) \cdots (p) = p!. \quad (\text{A17})$$

Relations (A16) and (A11) can now be used for computing the variance:

$$\begin{aligned} \sigma^2 &= E[V^2(x)] - \{E[V(x)]\}^2 \\ &= \frac{A}{N} - \frac{1}{N^2} - \frac{2A \text{sinc}(Ax)}{N\sqrt{N}} \rightarrow \frac{A}{N}, \end{aligned} \quad (\text{A18})$$

where we neglect a second-order term that compares with terms already neglected from the series expansion. The last approximation is valid for a relatively large number of identical input objects  $N$ . The above approximations were examined by computer simulations, and the functional dependence on  $(N, N^2, \dots)$  was verified. Note that the mean and the variance are position dependent unless a large number of objects are present.

For a large aperture  $A$  we may approximate  $A \text{sinc}(Ax)$  by a Dirac delta function. Hence, from relation (A12) we see that the mean of  $V(x)$  is large only near  $x = 0$  and negligible elsewhere, in particular for a large number of objects  $N$  in the input to which the filter is matched. Since the mean is nonzero at  $x \approx 0$  only, we compare the variance with the mean at  $x \approx 0$  and obtain

$$\frac{\sigma^2}{\langle V(x) \rangle} \approx \frac{A/N}{A^2/N} = \frac{1}{A}. \quad (\text{A19})$$

Hence, as the aperture size increases, this ratio decreases, implying a low normalized variance. This proves that  $V(x)$  is a narrow function with low variance when  $x_i$  is a uniformly distributed random variable.

## References and Notes

1. J. Rosen, T. Kotzer, and J. Shamir, "Optical implementation of phase extraction pattern recognition," *Opt. Commun.* **83**, 10-14 (1991).

2. O. K. Ersoy and M. Zeng, "Nonlinear matched filtering," *J. Opt. Soc. Am. A* **6**, 636-648 (1989).
3. O. K. Ersoy, Y. Yoon, N. Keshava, and D. Zimmerman, "Nonlinear matched filtering 2," *Opt. Eng.* **29**, 1002-1012 (1990).
4. T. Kotzer, J. Rosen, and J. Shamir, "Phase extraction pattern recognition," *Appl. Opt.* **31**, 1126-1137 (1992).
5. B. Javidi, "Generalization of the linear matched filter concept to nonlinear matched filters," *Appl. Opt.* **29**, 1215-1223 (1990).
6. F. T. S. Yu, F. Cheng, T. Nagata, and D. A. Gregory, "Effects of fringe binarization of multi-object joint transform correlator," *Appl. Opt.* **28**, 2988-2990 (1989).
7. M. H. Hayes, J. S. Lim, and A. V. Oppenheim, "Signal reconstruction from phase or magnitude," *IEEE Trans. Acoust. Speech Signal Process.* **ASSP-28**, 672-680 (1980).
8. M. H. Hayes, "Reconstruction from magnitude or phase," in *Image Recovery: Theory and Applications*, H. Stark, ed. (Academic, New York, 1987), pp. 195-230.
9. J. L. Horner and P. D. Gianino, "Phase-only matched filtering," *Appl. Opt.* **23**, 812-816 (1984).
10. B. Javidi, C.-J. Kuo, and S. F. Odeh, "Performance of a bipolar nonlinear correlator," in *Piece Recognition and Image Processing*, W. Wiitaner, ed., *Proc. Soc. Photo-Opt. Instrum. Eng.* **956**, 120-130 (1988).
11. After receiving the review of this paper we noticed that using this specific type of threshold in the binary JTC seems to be the thought behind the adaptive threshold employed by W. B. Hahn and D. L. Flannery, "Design elements of binary joint transform correlation and selected optimization techniques," *Opt. Eng.* **31**, 896-905 (1992). However, their threshold is only an approximation to the one obtained by Eq. (19), which is the only one to obtain true phase-only correlation.
12. B. Javidi and J. Wung, "Binary nonlinear joint transform correlation with median and subset median thresholding," *Appl. Opt.* **30**, 967-976 (1991).
13. S. D. Lindell and D. L. Flannery, "Ternary phase amplitude filters for character recognition," in *Optical Information Processing Systems and Architectures*, B. Javidi, ed., *Proc. Soc. Photo-Opt. Instrum. Eng.* **1151**, 174-182 (1989).
14. B. A. Kast, M. K. Giles, S. D. Lindell, and D. L. Flannery, "Implementation of ternary phase amplitude filters using a magneto-optic spatial light modulator," *Appl. Opt.* **28**, 1044-1046 (1989).